Research Article | Vol. 32, No. 15 / 15 Jul 2024 / Optics Express 25789
Optics EXPRESS

Hump-shaped seven-core fiber-based WaveFlex biosensor for rapid detection of glyphosate pesticides in real food samples

QI ZHANG,[1] CHAOFAN GU,[1] RAGINI SINGH,[2] SOURABH JAIN,[3] RAY T. CHEN,[4] BINGYUAN ZHANG,[1,6] AND SANTOSH KUMAR[1,5,7]

[1]*Shandong Key Laboratory of Optical Communication Science and Technology, School of Physics Science and Information Technology, Liaocheng University, Liaocheng 252059, China*
[2]*Department of Biotechnology, Koneru Lakshmaiah Education Foundation, Vaddeswaram, Andhra Pradesh – 522302, India*
[3]*Microelectronics Research Center, The University of Texas at Austin, Austin, TX 78758, USA*
[4]*Department of Electrical and Computer Engineering, The University of Texas at Austin, Austin, TX 78705, USA*
[5]*Centre of Excellence for Nanotechnology, Department of Electronics and Communication Engineering, Koneru Lakshmaiah Education Foundation, Vaddeswaram, Andhra Pradesh–522302, India*
[6]*zhangbingyuan@lcu.edu.cn*
[7]*santosh@kluniversity.in*

Abstract: At present, pesticides are widely used in the cultivation of crops. Glyphosate is widely used in many pesticides. Glyphosate ingestion can cause a series of health problems. Therefore, this paper proposes to use localized surface plasmon resonance (LSPR) technology to develop a WaveFlex biosensor (plasma wave-based optical fiber sensor) to detect glyphosate concentration in pesticides. The evanescent field is improved by using the fusion of seven-core fiber and single-mode fiber and the tapering of the sensing area to improve the sensing performance. The gold nanoparticles (AuNPs) are used to excite the LSPR effect. Multi-walled carbon nanotubes (MWCNTs) and cerium oxide nanorods (CeO_2-NRs) are used to increase the surface area and promote the adhesion of the enzyme. The sensitivity of the sensor is 137.7 pm/μM in the range of 0-60 μM glyphosate concentration, and the limit of detection (LoD) is 1.94 μM, which has good performance in compared to the existing biosensors. Subsequently, the sensor was tested for reusability, reproducibility, selectivity, stability, and excellent results were obtained. Finally, the sensor is tested on real samples, and the results show that it can be applied in practical applications. The test findings demonstrate that the sensor has a great deal of potential for use in glyphosate content detection in food samples.

1. Introduction

Monitoring food safety is crucial for the safety and well-being of human life, as well as for promoting sustainable social and economic growth. The issue of food safety has attracted more and more attention in recent years. As the source of food, the production process is particularly important. Pesticide residues are the most important food hazards in the production process and the biggest problem of food safety [1]. The unreasonable use and residue of pesticides pose a great threat to people ‘s health. Intake of food containing pesticide residues may lead to acute and chronic poisoning, causing cancer, neurasthenia and other diseases [2,3]. Moreover, pesticide residues can cause serious pollution to the environment [4]. Although the use of pesticides can cause many harms, the non-use of pesticides will reduce crop yields and bring diseases and pests to crops [5]. Therefore, it is imperative to develop a tool for detecting pesticide residues.

Among many pesticides, glyphosate is widely used because of its broad spectrum and selectivity [6]. However, glyphosate has the characteristics of extremely soluble in water [7], and has a long

#530348 https://doi.org/10.1364/OE.530348
Journal © 2024 Received 16 May 2024; revised 21 Jun 2024; accepted 24 Jun 2024; published 2 Jul 2024

Optics EXPRESS

half-life in water, so it will flow with the water to various places, causing great harm to aquatic ecosystems and humans. Glyphosate mainly binds to the 5-enolpyruvylshikimate-3-phosphate synthase (EPSP) enzyme in plants [8], thereby inhibiting its catalytic reaction and causing plants to fail to synthesize amino acids normally. It affects protein synthesis, which also leads to the lack of basic materials for life activities in plants. Plants cannot grow and develop normally, and eventually die. The harm of glyphosate to the human body is mainly through the inactivation of acetylcholinesterase in the human body [9], resulting in the weakening of the human nervous system, resulting in respiratory system, metabolic system and other dysfunction [10]. Some studies have also pointed out that glyphosate is metabolized to carbamate (AMPA) and so on [11]. AMPA can adversely affect the mitochondrial function and DNA synthesis of cells, and may be related to some potential cytotoxicity, mutagenicity and carcinogenicity [12,13]. The World Health Organization (WHO) states that there is no more than 5.32 μM of glyphosate in drinking water [14]. Therefore, a biosensor for the detection of trace glyphosate can be developed to rapidly detect the concentration of glyphosate in water and crops to contribute to human health.

At present, methods such as Gas Chromatography [15], (High Performance Liquid Chromatography) HPLC [16], (Enzyme-Linked Immunosorbent Assay) ELISA [17], (Inductively Coupled Plasma Mass Spectrometry) ICP-MS [18] and electrochemical sensor [19] are mainly used to detect glyphosate. Because glyphosate has the characteristics of extremely soluble in water, long half-life, and poor fluorescence absorption [20], traditional methods require pretreatment. Methods such as HPLC require high-end equipment and professional skills. Different from the above methods for detecting glyphosate, fiber-based biosensors have the characteristics of simple operation, small size, and no pretreatment, and their excellent anti-electromagnetic interference characteristics can reduce the impact of the surrounding environment [21]. Zhang *et al*. proposed a biosensor based on U-shaped fiber for the detection of acetylcholine, which has high sensitivity [22]. Singh *et al*. developed a LSPR-based biosensor using gold nanoparticles (AuNPs) and MXene materials to detect tyramine concentration [23], with a detection limit of 6.96 μM. It can be seen that the fiber-based biosensor has high sensitivity and excellent detection limit, which is very suitable for detecting trace glyphosate.

Localized surface plasmon resonance (LSPR) technology is an optical sensing technology based on the surface plasmon resonance effect of metal nanoparticles (MNPs). When the frequency of the incident light is consistent with the frequency of the free electron oscillation in the MNPs, the interaction leads to the collective oscillation of the surface electrons [24], triggering the resonance phenomenon. In the field of biosensors, LSPR technology has the advantages of excellent catalytic performance, label-free, and good biocompatibility [25,26], reducing potential interference factors. Good biocompatibility enables nanomaterials to interact with substances without causing significant toxicity or damage [27]. In this way, LSPR technology can be applied in the fields of biomolecular interaction and material recognition. According to the relevant literature, the use of nanomaterials can enhance the resonance effect of biosensors [28], which can better to detect the interaction of biomolecules.

In recent years, nanomaterials have flourished for the development of agricultural biosensors. Multi-walled carbon nanotubes (MWCNTs) have become one of the hot research topics due to their outstanding physical and chemical properties [29]. MWCNTs have excellent electrical conductivity [30,31], allowing electrons to flow unimpeded inside, thereby achieving high electrical conductivity. MWCNTs also have high chemical stability [32], which can resist oxidation and corrosion of many chemicals, so they can be durable. These properties make them widely used in the field of sensors. Every year, the world produces abundant cerium rare earth metals [33], a large number of which are made into cerium oxide nanoparticles (CeO_2-NPs). It can be seen that CeO_2-NPs have become popular nanomaterials. Similarly, cerium oxide nanorods (CeO_2-NRs) exhibit good thermal stability at high temperatures [34,35], which makes it not affected by ambient temperature. In the material interaction, CeO_2-NRs has high sensitivity

Optics EXPRESS

[36], which can effectively promote the interaction between molecules adsorbed on its surface. The above two nanoparticles (NPs) have high specific surface area and abundant surface-active sites, which can effectively enhance the intensity of LSPR resonance signal. This surface enhancement effect can improve the sensitivity and detection limit of the sensor, so that the LSPR technology can detect low concentration target molecules. In addition, MWCNTs can be used as an adsorbed CeO_2-NRs platform because it has a conjugated structure showing a strong hydrophobic surface [37]. The coupling of MWCNTs and CeO_2-NRs is the combination of metal oxides and carbon-based materials, which is conducive to the improvement of sensing performance [38].

In this work, a hump-shaped WaveFlex biosensor was developed using single-mode fiber (SMF) and seven-core fiber (SCF). The sensor is based on the LSPR principle and uses AuNPs to excite the resonance effect. MWCNTs and CeO_2-NRs were used to characterize the fiber to improve the sensing performance. Finally, the performance of the sensor is evaluated. The selectivity, repeatability, stability, reusability and pH of the sensor were tested. The sensitivity of the sensor is 137.7 pm/μM, the limit of detection (LoD) is 1.94 μM .The results showed that the sensor had a significant effect on the detection of trace glyphosate.

2. Experiments

2.1. Materials and reagents

The hump-shaped fiber is made of single-mode fiber (SMF, 9/125 μm) and seven-core fiber (SCF, 6.1/125 μm), purchased from Shenzhen, China and the United Kingdom, respectively. AuNPs were synthesized using tetrachloroauric acid ($HAuCl_4$) and sodium citrate. The fiber was washed with acetone, Piranha solution and deionized water, respectively. AuNPs were immobilized by (3-mercaptopropyl) trimethoxysilane (MPTMS). N, N-dimethylformamide (DMF) solution was used to prepare MWCNTs solution, and N-methyl-2-N-pyrrolidone (NMP) solution was used to prepare CeO_2-NRs solution. Glyphosate was purchased from McLean, China, and horseradish peroxidase (HRP) was purchased from Sigma-Aldrich, Shanghai. Paraoxon, 2,4-dichlorophenoxyacetic acid, lindane and atrazine were purchased locally.

2.2. Instruments and measurements

In order to make the sensor's high precision and accuracy, the sensor is developed by high precision instrument. The fiber optic fusion splicer machine (FSM, Japan) was used to fuse SMF and SCF, and the 3SAE combiner manufacturer system (CMS, USA) was used to taper the hump-shaped fiber. The absorption peak of AuNPs was determined by UV-Visible spectrophotometer (Hitachi-3310) to determine the morphology of nanoparticles. The microscopic distribution of NPs was observed by high resolution transmission electron microscopy (HR-TEM). The nanoparticle coating on the fiber surface was characterized by scanning electron microscopy (SEM).

2.3. Sensing principle of the probe

When light is incident from the optically dense medium to the optically sparse medium, total internal reflection (TIR) occurs when the incident angle exceeds the critical value. When the light has completed TIR at the interface between the cladding and the core, a small part of the light will pass through the interface and then propagate back to the core along the interface between the core and the cladding. In this process, part of the energy will pass through the boundary in a very short time and decay rapidly in the region near the boundary. This optical field is called the evanescent field, and the generated wave is called the evanescent wave (EWs). The evanescent field can excite the LSPR effect with AuNPs on the surface of the fiber, resulting in an absorption peak related to the refractive index (RI) [39]. However, the energy in the evanescent field extends

Optics EXPRESS

to the medium in the form of exponential decay, and decays to almost no energy after a certain distance from the boundary. This distance is called penetration depth defined as [40]:

$$d_p = \frac{\lambda}{2\pi\sqrt{n_{co}^2 sin^2\theta - n_{cl}^2}} \tag{1}$$

Here, d_p is the penetration depth, λ is the incident wavelength, n_{co} is the RI of the core, n_{cl} is the cladding RI, θ is the incident angle of light at the interface between the cladding and the core. Moreover, it is difficult for traditional optical fibers to generate strong evanescent fields, which limits the development of sensors. There are two main methods to improve the evanescent field: (i) fiber fusion with different core diameters and (ii) core diameter thinning. In this work, SMF-SCF-SMF and tapering of the fiber core, both are used to increase the evanescent field to improve the sensing performance. The proposed hump shaped WaveFlex fiber structure and optical field propagation is shown in Fig. 1.

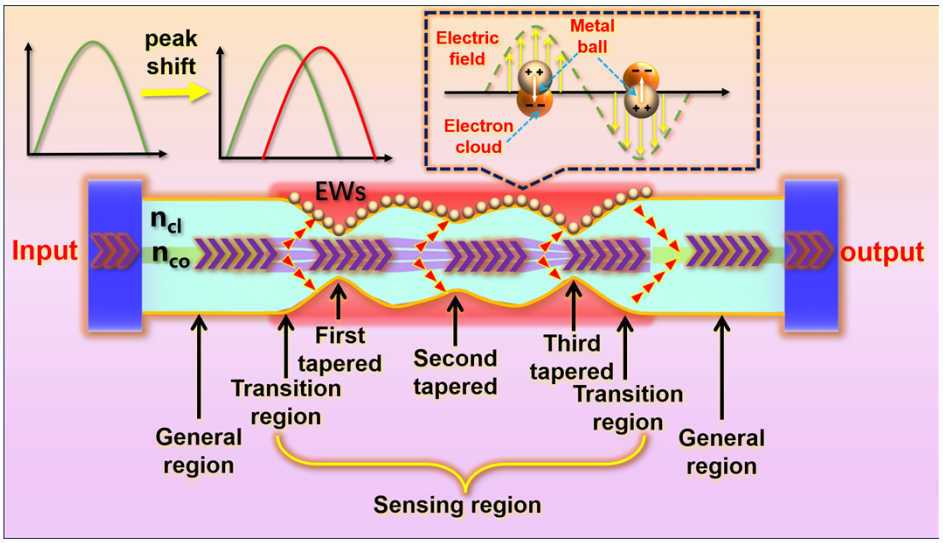

Fig. 1. The schematic diagram of hump-shaped optical fiber biosensor principle.

When light enters into SCF from SMF, a part of light enters into the central core of SCF. One part of the light entering the central core is transmitted along the core as the fundamental mode, and the other part of the light excites higher-order modes to enhance the evanescent field. The rest part enters the other six cores of SCF due to refraction. Due to the mismatch between the cores of SCF and SMF, the high-order modes of the six vertex cores of SCF regular hexagon are excited [41]. Since the central core is different from the other six core modes, mode interference will be generated, resulting in reduced coupling [42] and more evanescent waves. Therefore, the LSPR effect is stronger and the ability to detect the surrounding environment becomes stronger. Tapering the SCF in the fiber sensing area will make the cladding and core thinner, stimulate higher-order modes, produce more EWs [43], and further enhance the evanescent field.

HRP is an enzyme extracted from the roots of horseradish. It is a member of the peroxidase family. HRP is a commonly used enzyme in biosensor research because it retains its activity over a wide pH and temperature range [44]. HRP can catalyze the oxidation of many substances, and its main active group is a heme molecule containing iron [45]. According to the relevant literature, it is pointed out that HRP has an inhibitory effect on glyphosate, and the principle is that HRP reacts with the amine, carboxyl, and phosphine groups of glyphosate [46].

Optics EXPRESS

When the frequency of the incident light is consistent with the resonance frequency of AuNPs, the interaction between the electron cloud and the metal core produces the LSPR effect, resulting in a peak related to RI. When glyphosate inhibits the enzymatic reaction of HRP, the RI of the medium around the sensing area changes, resulting in the shift of the peak. The peak displacement can be expressed as [47]:

$$\Delta\lambda = m\Delta n_m \left(1 - e^{\frac{-2d}{d_p}}\right) \tag{2}$$

Here, $\Delta\lambda$ is the peak displacement, m is the sensitivity of AuNPs to the electromagnetic field, Δn_m is the variation of the surrounding medium RI, d is the thickness of the adsorption layer, and d_p is the penetration depth of EWs.

2.4. Simulation of sensor probe

The RSoft software's beam propagation method (BPM) is chosen to simulate light propagation in hump-shaped optical fibers in order to better comprehend the transmission characteristics and energy distribution of optical fibers. The SMF has a core diameter of 8.2 µm and a cladding diameter of 125 µm. The external environment's RI is set at 1. Fig. 2(a) displays the results of the simulation. "1, Launch" in the diagram denotes the light source's overall energy distribution, "1, Mode 0" the fiber core's energy distribution, and "2, Mode 0" the cladding's energy distribution. It can be seen from the diagram that when the light passes through the tapered area, the energy of the fiber core is significantly reduced. This is because part of the energy enters the cladding, resulting in a significant increase in the energy of the cladding. It can be seen that after the tapering of the sensing area and the fusion of optical fibers with different core diameters, the cladding energy is significantly increased, and the evanescent field is significantly enhanced. The simulation results showed that the evanescent field has been significantly increased. We simulated the structure without tapering, as shown in Fig. 2(b). It can be seen that compared with the structure without tapering, the taper cladding energy of the hump-shaped structure increases by 0.4 and 0.2. More cladding energy will excite more evanescent fields. Therefore, the hump-shaped structure is more excellent.The SCF has a core diameter of 6.1 µm and a cladding diameter of 125 µm. The length of the SCF is 25 mm, and the distance between the adjacent tapered waist is 10 mm. The cross-section of the seven-core fiber is shown in Fig. 2(c). The core spacing of the seven-core fiber is 35 µm.

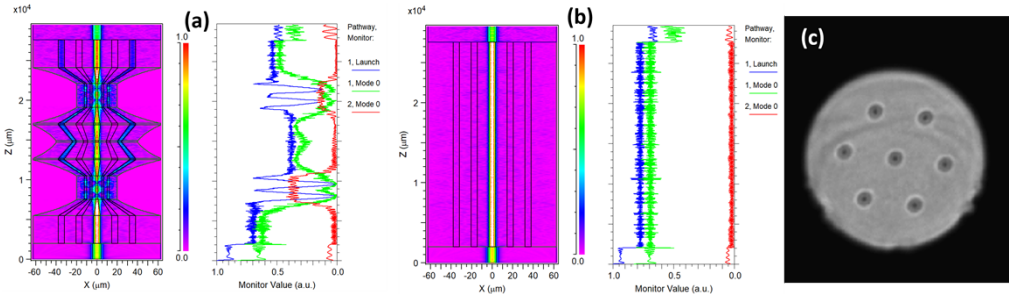

Fig. 2. (a) RSoft simulation results of proposed hump-shaped fiber structure, (b) RSoft simulation results of structure without tapering,(c) the cross-section of the seven-core fiber.

2.5. Fabrication process of the sensor probe

The sensing probe of the sensor is a combination of SMF and SCF. The combination of SMF and SCF can significantly improve the coupling efficiency and stimulate more cladding modes [48]. The distribution of SCF core is regular hexagon. One core is in the center of the regular hexagon,

Optics EXPRESS

and the remaining six cores are on the vertices of the regular hexagon. The cladding diameter of SCF is 125 µm, and the diameter of each core is 6.1 µm. The welding process is divided into two steps. In the first step, the coating layers of SMF and SCF are removed by a fiber optic stripper. SMF-SCF was formed by fusing FSM as shown in Fig. 3(a). In the second step, the formed SMF-SCF and another SMF are repeated to remove the coating layer and wipe. Finally, SMF-SCF and SMF are placed at both ends of the fiber fixture respectively and fused to form SMF-SCF-SMF. The SCF portion of the fused SMF-SCF-SMF was tapered using CMS as shown in Fig. 3(b). Before using CMS to taper the fiber, it is wiped with ethanol to avoid the influence of impurities on the taper treatment and the vacuum environment of CMS. CMS uses three-electrode discharge to taper the fiber. Through a large number of adjustments of discharge power, vacuum value, running speed and so on, the hump-shaped structure was gradually optimized, and finally a beautiful curve structure was obtained. The tapering process is divided into two steps, and the production process is shown in Fig. 3(c).

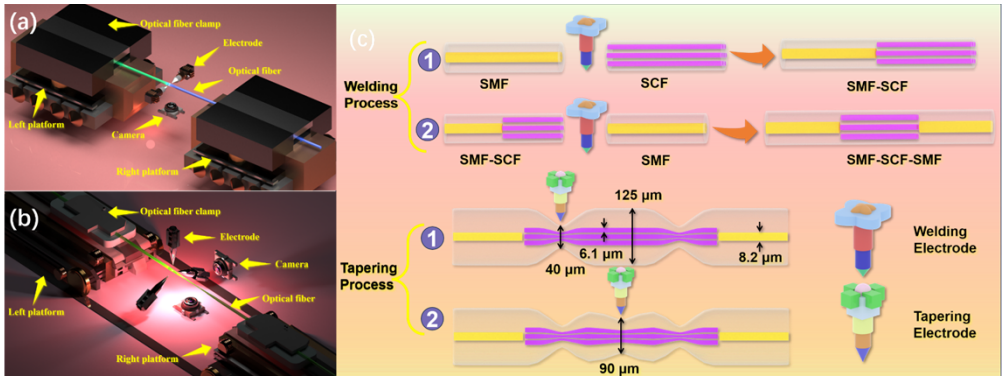

Fig. 3. (a) Schematic of FSM, (b) internal view of CMS, and (c) fabrication process of hump shaped WaveFlex fiber structure.

2.6. *AuNPs/MWCNTs/CeO_2-NRs synthesis process*

AuNPs with a diameter of about 10 nm were synthesized by the traditional Turkevich method [49] to excite the LSPR effect. The test tube was filled with 14.85 mL deionized water and added with tetrachloroauric acid solution. Heat to boil, turn on the rotation, and add trisodium citrate. Turn off the heat for 5 minutes and continue to rotate for 10 minutes. The solution appears wine red, which is the synthetic target of AuNPs. For MWCNTs solution, add 5 mg MWCNTs powder to 10 mL DMF solution, place it in an ultrasonic machine for 1 hour, and let it stand until the supernatant appears. For CeO_2-NRs solution, 17 mg of CeO_2-NRs powder was put into 8 mL of NMP solution and sonicated for 2 hours. Finally, it can be used in a centrifuge for 30 minutes.

2.7. *Nanomaterials immobilization*

AuNPs were fixed in the optical fiber sensing area to complete the LSPR effect. MWCNTs and CeO_2-NRs were fixed on the surface of the fiber to improve the sensing performance. The nanomaterials-immobilization process over fiber structure is shown in Fig. 4. The sensing area of the optical fiber is cleaned with acetone solution to remove impurities on the surface.

Then it was immersed in the Piranha solution, which was composed of 30% H_2O_2 and H_2SO_4 in a ratio of 3:7 for 30 minutes. The fiber was rinsed with deionized water and dried with N_2 to remove excess Piranha solution. After hydroxylation, the optical fiber sensing area was immersed in MPTMS solution for 12 hours to form SH functional group. Then the optical fiber sensing area was placed in the prepared AuNPs solution for 48 hours. The fiber was rinsed with ethanol

Optics EXPRESS

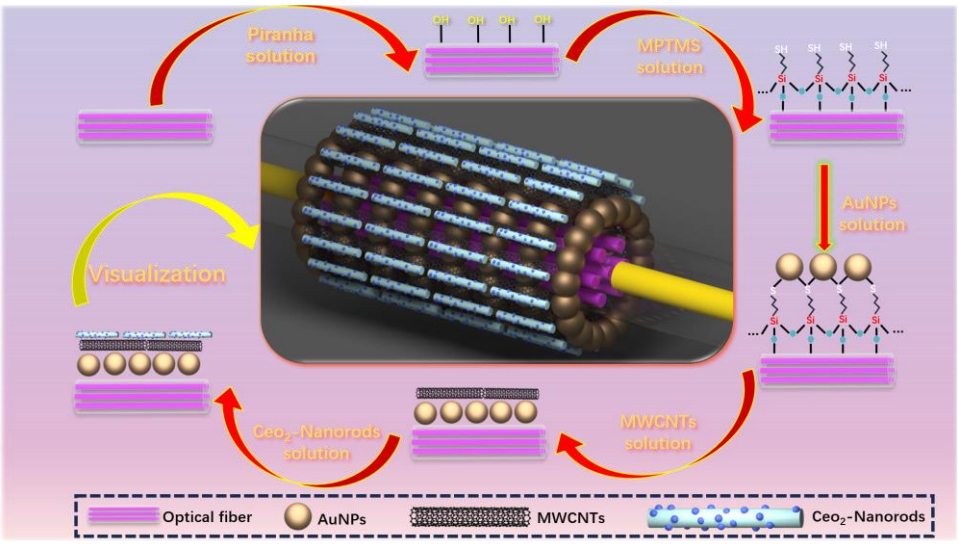

Fig. 4. Schematic view of nanoparticles immobilization process on the hump-shaped optical fiber structure.

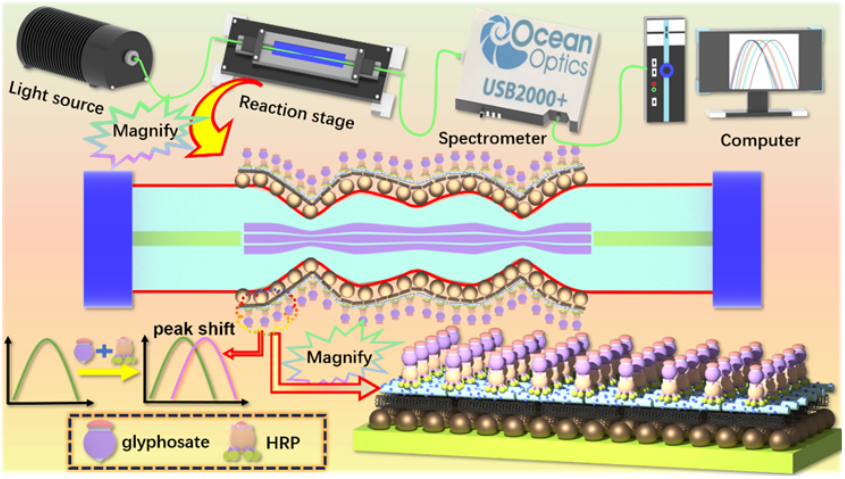

Fig. 5. Experimental setup for the measurement of glyphosate solution through the hump shaped WaveFlex biosensor.

to remove unbounded AuNPs. Thereafter, MWCNTs and CeO_2-NRs were re-immobilized. Then, optical fiber sensing area was first immersed in MWCNTs solution for 10 minutes, and then placed in an oven for 20 minutes at 70°C. The above operations were repeated three times to determine the immobilization of MWCNTs on the fiber. Thereafter, optical fiber sensing area was immersed in CeO_2-NRs solution for 10 minutes and placed in an oven at 70°C for 20 minutes. Repeated these steps 3 times for uniform coating of nanomaterials over the fiber surface.

2.8. Preparation of glyphosate solutions

An electronic scale was used to precisely weigh 5.07 mg of glyphosate powder. To generate a stock solution with a 1000 µM concentration of glyphosate, the powder was fully dissolved in 30 mL of 1×PBS solution (pH 7.4). Thereafter, eight distinct concentrations of glyphosate solution

Optics EXPRESS

were prepared by diluting the stock solution with PBS solution in order to assess the viability of the sensor to detect trace glyphosate molecules.

2.9. Experimental setup for glyphosate measurement

The tungsten-halogen light source (HL-2000, Ocean Optics, USA), spectrometer (USB2000+, Ocean Optics, USA), optical fiber fixture and structure, measurement solution, and computer make up the complete experimental apparatus. Firstly, the light source transmission line is fused with the optical fiber, and then the other end of the optical fiber is fused with the spectrometer transmission line, and then the spectrometer is connected to the computer by USB. Here, the enzymatic reaction of HRP is inhibited by glyphosate, resulting in a change in the peak, and the changed spectrum can be observed by a computer. The glyphosate concentration information can be obtained according to the peak change of the spectrum. In Fig. 5, the experimental apparatus is displayed.

3. Results and discussions

3.1. Optimization of the sensor probe

SCF is the sensor's main sensing region. As such, it is especially crucial to optimize the sensor's SCF length. Thus, five sensors were fabricated, each having a distinct SCF length. Subsequently, the transmission intensity is measured, and Fig. 6(a) displays the results. Here, the 25 mm SCF structure has the lowest transmission intensity, means, more EWs are generated, which is advantageous for the detection of drugs at lower concentrations. Thus, the SCF length of 25 mm was chosen for development of proposed sensor probe. The sensing area of the spliced fiber is tapered to further improve the evanescent field and improve the sensing performance. Wang *et al*. made a new type of sensor using two hump-shaped tapers to measure the bending direction and temperature, and obtained good results [50]. In addition, the increase of the hump will cause the fiber structure to become thinner and even lead to breakage during the experiment. Reducing the hump will lead to a decrease in EWs and a decrease in sensing performance. Based on the literature and the above reasons, three tapered regions are selected to form a hump-shaped fiber structure. The hump-shaped curve has high tapered area and low tapered area.For the low tapered, the smaller the taper diameter, the lower the transmission strength. More light penetrates into the cladding to enhance the evanescent field. However, the smaller the taper diameter, the easier it is to break in the fixation process and measurement experiments. For the high tapered, the higher the diameter of the tapered area leads to the decrease of EWs. The lower the diameter of the tapered area leads to the decrease of flexibility. After multiple debugging of the curve and flexibility investigation, 40 µm and 90 µm were selected to make the hump-shaped fiber structure [51]. The direct scanning diagram of the hump-shaped fiber structure is shown in Fig. 6(b). The normalized transmission intensity is shown in Fig. 6(c). The SD was calculated to be 0.1725.The results show that the fabricated hump-shaped optical fiber has a high degree of repeatability, which ensures the stability of the experimental results.

3.2. Characterization of nanomaterials

The absorption spectra of the synthesized AuNPs were measured by UV-visible spectrophotometer. The results are shown in Fig. 7(a), and the peak of the absorption spectrum was 519 nm. The results show that the diameter of the synthesized AuNPs is about 10 nm. The synthesized AuNPs were characterized by HR-TEM. The results are shown in Fig. 7(b), and the appearance of the synthesized AuNPs is spherical and the diameter is uniform. The characterization results of MWCNTs and CeO_2-NRs are shown in Figs. 7(c) and (d), respectively.

Optics EXPRESS

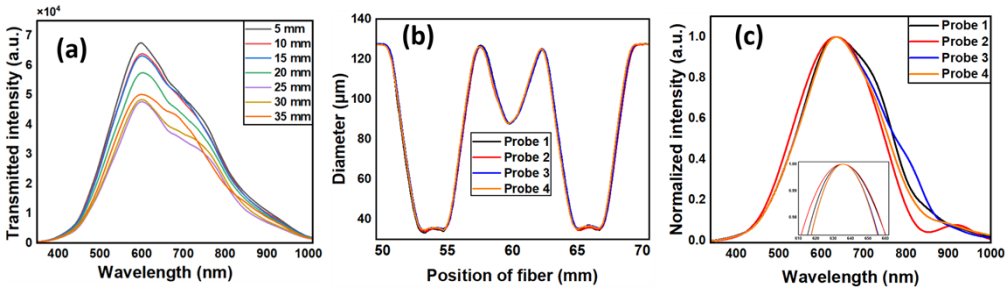

Fig. 6. (a) SCF length optimization, (b) hump-shaped fiber diameter scanning diagram, and (c) hump-shaped fiber normalized intensity spectrum.

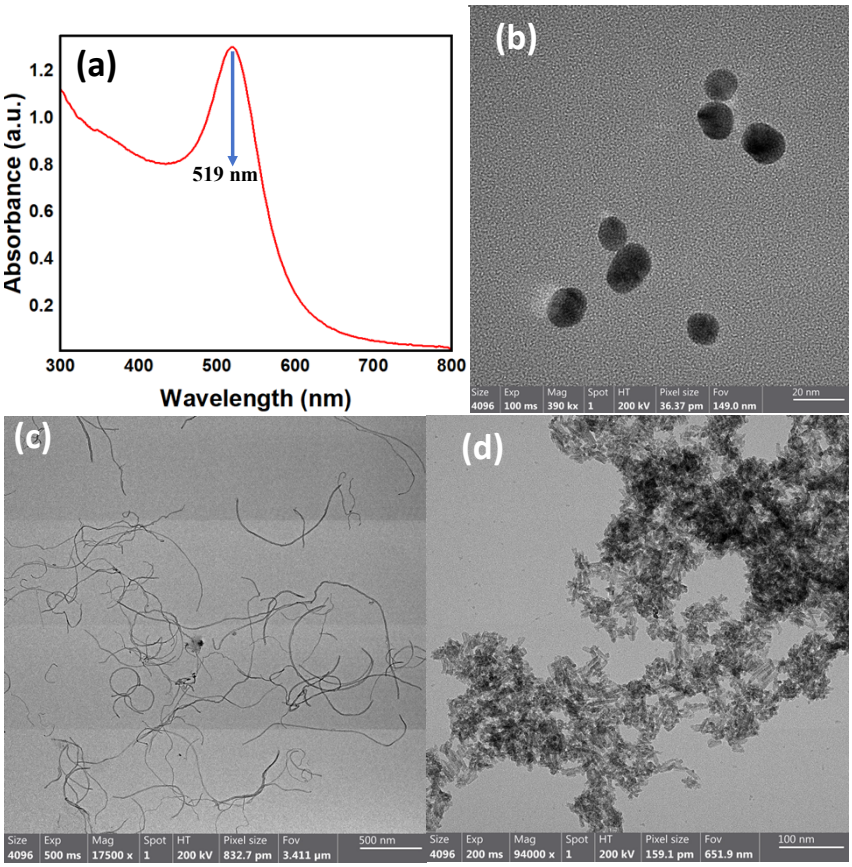

Fig. 7. (a) Absorbance spectrum of AuNPs, and HR-TEM images of (b) AuNPs, (c) MWCNTs and (d) CeO_2-NRs.

Optics EXPRESS

3.3. Characterization of the nanomaterials-immobilized structure

The structure of the fiber and the NPs on the surface of the fiber were observed by precise SEM. The results of the fiber structure are shown in Fig. 8(a), and the taper regions at both ends and in the middle of the fiber can be clearly seen. The NPs on the surface of the fiber are shown in Fig. 8(b). It can be seen that AuNPs are evenly distributed on the surface of the fiber as small particles. Then MWCNTs and CeO_2-NRs can be seen. The elements on the surface of the fiber were analyzed by SEM-EDS, which further proved that the above three NPs existed on the surface of the fiber. The results are shown in Fig. 8(c). The presence of Au, Ce, C and O on the surface of the fiber confirmed the presence of AuNPs, MWCNTs and CeO_2-NRs on the fiber.

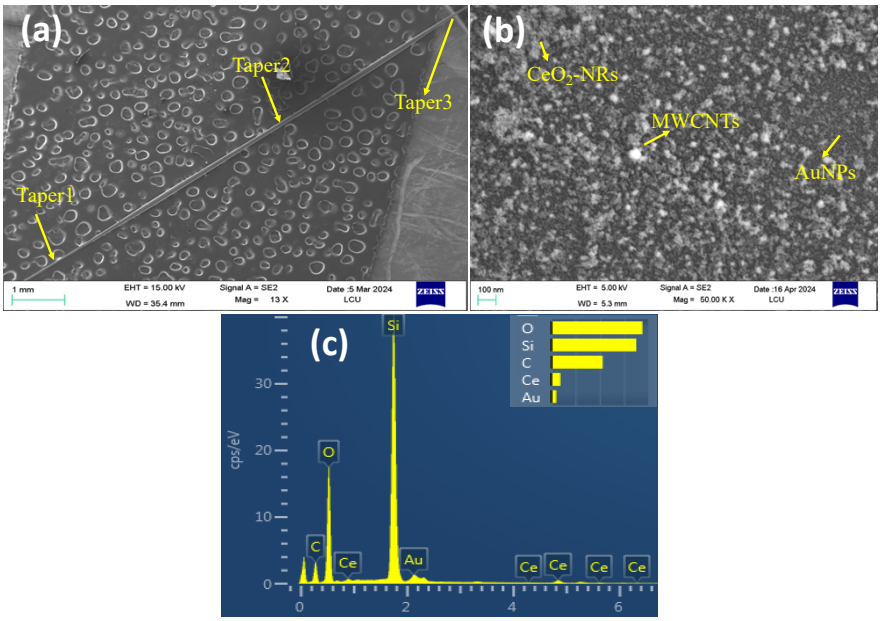

Fig. 8. (a) SEM image of optical fiber surface, (b) SEM image of nanoparticles on optical fiber surface, (c) EDS analysis of Fig. 8(b).

3.4. Measurement of glyphosate solutions

Eight different concentrations of glyphosate solutions were prepared and measured using the device shown in Fig. 5. The solution of 0 μM was added first, and the spectrum was recorded after the LSPR spectrum was stable. The measurement sequence was from low concentration to high concentration, and 1 × PBS solution was used to rinse during the measurement to reduce the influence of each concentration. The LSPR spectrum of the solutions were recorded by measuring the different glyphosate concentration, as shown in Fig. 9(a). With the increase of glyphosate concentration, the LSPR spectral peak red shifted. The more the glyphosate concentration increases, the more the LSPR spectrum peak wavelength shifts. An analysis was conducted to determine the correlation between the glyphosate concentration and the peak wavelength shift of the LSPR spectrum, as shown in Fig. 9(b). The linear fitting equation is:

$$\lambda = 0.13774\ C + 634.425 \tag{3}$$

Here, C denotes the concentration of glyphosate, corresponding to the abscissa. λ represents the peak wavelength of the LSPR spectrum, corresponding to the ordinate. The fitting degree R^2 is 0.99, indicating that the designed sensor has high linearity and high feasibility.

Optics EXPRESS

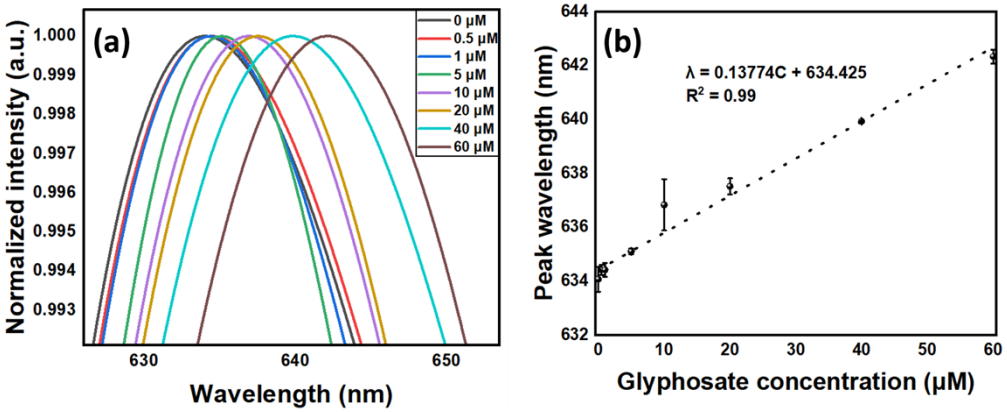

Fig. 9. (a) Sensing spectrum, (b) linearity result of sensor.

Combining Eq. (2), the relationship between the RI of the surrounding medium and the glyphosate concentration can be obtained as follows [52]:

$$0.13774\ C = m\Delta n_m \left(1 - e^{\frac{-2d}{dp}}\right) \tag{4}$$

Sensitivity is another crucial metric for assessing the sensor's performance. It is the ratio of the peak wavelength change value to the glyphosate concentration change value, and it shows the slope of the linear fitting line. According to Fig. 9(b), the sensitivity is 137.7 pm/μM, indicating that the sensor has a high sensitivity to glyphosate concentration. In order to evaluate whether the sensor can detect trace glyphosate concentration, the detection limit is an important indicator. The detection limit refers to the minimum concentration of the target analyte detected by the sensor, and the calculation formula is:

$$\mathrm{LOD} = \frac{3 \times SD}{S} \tag{5}$$

Here, S represents the sensitivity of the sensor. The SD is the standard deviation of the measured fifteen peak wavelengths, and the SD value is 0.089.

According to the calculation, the LOD is 1.94 μM, which is lower than the 5.32 μM specified by the WHO. It can be seen that the sensor has the ability to detect trace glyphosate concentration.

3.5. Stability and pH Test

The stability experiment can test the performance stability of the sensor during long-term operation. Under the same environmental conditions, the peak wavelength of 1×PBS solution was measured continuously for fifteen times at the same time interval. The outcomes are displayed in Fig. 10(a). Over a long period of time, the sensor fluctuates less. It is evident from the computed SD is that the sensor has high stability.

By evaluating the performance of the sensor under specific pH conditions, we can better understand the effect of external environment in practical applications. The 1×PBS can effectively buffer the pH value of the solution, keep it stable within a certain range, and easily adjust the pH value. Therefore, 1×PBS (pH = 7.4) was used as the buffer solution and one of the pH environments for the test. The pH of the buffer solution was adjusted to 3 by acetic acid reagent, 6 by ethanol reagent, and 10 and 13 by sodium hydroxide reagent. Glyphosate concentrations of 0 μM and 60 μM were redetected in the order from low to high. The difference is calculated to better observe the data. The measurement results are shown in Fig. 10(b), and the difference is

Optics EXPRESS

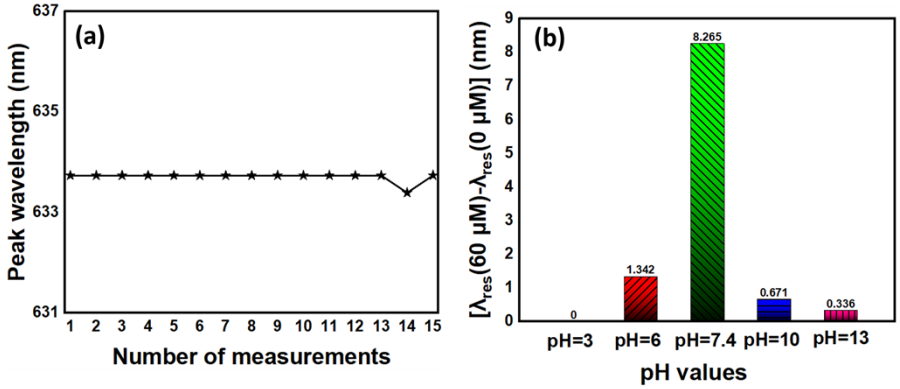

Fig. 10. (a) Stability, (b) pH test of developed sensor.

the largest when the pH is 7.4. Therefore, 1×PBS solution was selected as the pH environment of this experiment.

3.6. Reproducibility and Reusability Test

The reliability of the sensor can be verified by reproducibility experiments. If different sensors get the same sensing results in the same environment, it can be considered that the sensor is credible. Two different sensors made in the same batch were used to measure 60 μM glyphosate solution to test the reproducibility of the sensor. The reproducibility results are shown in Fig. 11(a). The SD was calculated to be 0.243, which proves that the sensor has good reproducibility.

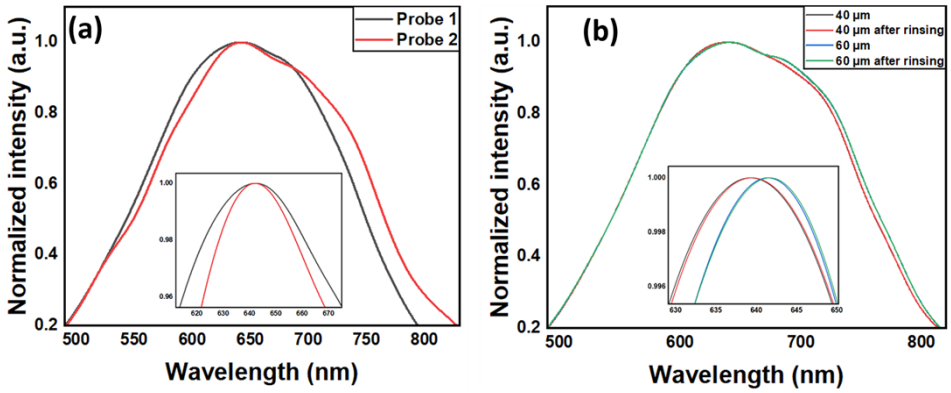

Fig. 11. (a) Reproducibility, (d) reusability results of developed sensor.

Reusability is also an important indicator to test the reliability of the sensor. The same sensor measures the same target analyte twice, and the experimental results are the same, indicating that the sensor has good reusability. In order to verify the reusability, 40 μM and 60 μM glyphosate solution solutions were measured twice. During the second measurement of the same solution, the optical fiber was rinsed with 1×PBS solution to reduce interference. The results are shown in Fig. 11(b). After calculation, the SD corresponding to 40 μM and 60 μM is 0, indicating that the sensor has good reusability.

Optics EXPRESS

3.7. Selectivity test

Selectivity is the ability to evaluate the sensitivity of the sensor to the target substance. Paraoxon, atrazine, 2,4-dichlorophenoxyacetic acid and lindane were selected as interfering substances. The difference between the peak wavelengths of the highest point 60 μM and the lowest point 0 μM in the linear range was measured. The results are shown in Fig. 12. When the measured substance is glyphosate, the peak wavelength displacement is the largest, and the displacement of other substances is very small. The results showed that the enzymatic reaction of glyphosate to HRP was specific, which further indicated that the sensor had high selectivity to glyphosate. The selected interfering substances are all present in pesticide residues. By simulating the interfering substances in the actual application scenario, the selectivity and anti-interference ability of the sensor to different interfering substances can be evaluated to guide the application of the sensor in the interference environment.

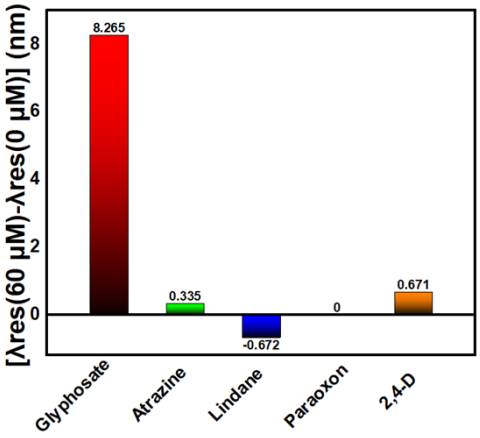

Fig. 12. Selectivity test results of developed sensor.

3.8. Real sample

The real sample experiment was carried out in the actual environment, which can better reflect the performance of the sensor. Because glyphosate that is mainly found in crops, soybeans and corn were selected as real samples for testing. Mash the corn, then put it into 1×PBS solution, stand for a period of time, take the supernatant used. Soybean repeat the above operation. Finally, the glyphosate solution was added to the real sample for measurement. The results are displayed in Table 1, and the recovery rate does not fluctuate much, indicating that the real sample measurement results of the sensor are almost consistent with the test results. The RSD was lower, indicating that the difference between the three experimental results was lower. Through this experiment, it is proved that the sensor has good strength in determining real samples.

Table 1. Determination results and recoveries of glyphosate in real samples

Sample	Recovery (%)	RSD (%) (n = 3)
Corn	83.3%-100.0%	5.83%
Soya bean	91.6%-111.1%	5.78%

Optics EXPRESS

3.9. Performance study of the developed sensor

Nowadays, there are many methods to detect glyphosate. These techniques do, however, have certain drawbacks, including the need for specialized equipment, complicated operation, high cost, and extended detection times. The use of LSPR technology can avoid these shortcomings. The LSPR technology only needs simple optical equipment, such as light source, spectrometer, etc., to complete the detection of glyphosate, and the LSPR technology cost is low. The proposed sensor is contrasted with current sensors in Table 2 in terms of nanomaterials, techniques, linear range, sensitivity, and detection limit. As the table shows, it is evident that the proposed sensor has the advantages of high sensitivity, low detection limit and simple operation. Other sensors based on optical fiber structure to detect glyphosate generally have the characteristics of large volume, inability to be portable, and complicated production process [57,58]. However, the developed sensor required a small volume per device and is easy to carry. The sensor structure can be made by using a specific program, the production process is simple, and the cost is low. In addition, it also has good repeatability and stability. This provides a good sensing device for the detection of glyphosate.

Table 2. Performance comparation with existing glyphosate biosensors

Nanomaterials used	Mechanisms	Linear range(μM)	Sensitivity	LoD(μM)	Ref.
ZnO/CuO/Au	Electrochemical	6.9-230	n.r.[a]	0.35	[53]
ZnO-NPs/PDDA/ SPAGE	Electrochemical	0-5000	n.r.[a]	2.84	[54]
CDs/AuNCs	Fluorescence	0-0.18	n.r.[a]	4.19	[55]
Cu-TCPP/AuNPs/CP	Electrochemical	0.2-120	n.r.[a]	0.03	[12]
BTSC-CDs	Fluorescence	0.2-30	n.r.[a]	0.27	[56]
AuNPs/MWCNTs/ CeO_2	LSPR	0-60	137.74 pm/μM	1.94	This work

[a]not reported

4. Conclusion

In this study, the concentration of glyphosate was determined using a fiber optic biosensor based on LSPR technology. FSM is used to fuse SMF-SCF-SMF to improve the evanescent field. The CMS is used to taper the fiber to form a hump-shaped cone area, which further improves the evanescent field and improves the sensing performance. MWCNTs and CeO_2-NRs were used to promote the reaction of glyphosate and HRP to improve the sensitivity. HR-TEM was used to observe three different nanoparticles, which verified the expected nanoparticles were synthesized. The nanoparticles on the fiber's surface were characterized using SEM, and the findings demonstrated that the nanoparticles were firmly affixed to the surface. Experimental results show that. In the range of 0-60 μM glyphosate concentration, the linear fitting degree is 0.99, sensitivity of 137.7 pm/μM, and detection limit of 1.94 μM, indicating that the designed sensor has good performance. The sensor's selectivity, pH value, stability, repeatability, and reusability were all tested. This series of excellent results show that the sensor has a bright future in the detection of glyphosate. It shows great value in the detection of pesticide residues.

Funding. Special Construction Project Fund for Shandong Province Taishan Mountain Scholars; Liaocheng University (318052341); Science and Technology Support Plan for Youth Innovation of Colleges and Universities of Shandong Province of China (2022KJ107).

Disclosures. The authors declare no conflicts of interest.

Data availability. Data underlying the results presented in this paper are not publicly available at this time but may be obtained from the authors upon reasonable request.

Optics EXPRESS

References

1. M. Elmi, T. Ghane, B. Daraei, *et al.*, "Monitoring of pesticide residue in pistachio nut samples by LC/MS-MS," Food Chem. **437**, 137848 (2024).
2. N. A. Shad, A. Munawar, A. Rakha, *et al.*, "In-field deployable and facile nanosensor for the detection of pesticides residues," Anal. Chim. Acta **1259**, 341204 (2023).
3. J. Brinco, "Analysis of pesticide residues in soil: A review and comparison of methodologies," Microchem. J. **195**, 109465 (2023).
4. B. Ruomeng, O. Meihao, Z. Siru, *et al.*, "Degradation strategies of pesticide residue: From chemicals to synthetic biology," Synth. Syst. Biotechnol. **8**(2), 302–313 (2023).
5. S. Mohamadi, B. Akbari-adergani, P. Sadighara, *et al.*, "Quantitative analysis of multiclass pesticide residues in spinach, Iran," Appl. Food Res. **3**(2), 100368 (2023).
6. S. Wang, Y. Yao, J. Zhao, *et al.*, "A novel electrochemical sensor for glyphosate detection based on Ti_3C_2Tx/Cu-BTC nanocomposite," RSC Adv. **12**(9), 5164–5172 (2022).
7. Y. Yang, B. Ghalandari, and L. Lin, "A turn-on fluorescence sensor based on Cu^{2+} modulated DNA-templated silver nanoclusters for glyphosate detection and mechanism investigation," Food Chem. **367**, 130617 (2022).
8. J. S. Santos, M. S. Pontes, E. F. Santiago, *et al.*, "An efficient and simple method using a graphite oxide electrochemical sensor for the determination of glyphosate in environmental samples," Sci. Total Environ. **749**, 142385 (2020).
9. R. Balaji, V. Renganathan, C.-P. Chu, *et al.*, "Periodic copper microbead array on silver layer for dual mode detection of glyphosate," OpenNano **8**, 100105 (2022).
10. C. Zhang, Y. She, T. Li, *et al.*, "A highly selective electrochemical sensor based on molecularly imprinted polypyrrole-modified gold electrode for the determination of glyphosate in cucumber and tap water," Anal. Bioanal. Chem. **409**(30), 7133–7144 (2017).
11. W. Zhang, Y. Feng, L. Ma, *et al.*, "A method for determining glyphosate and its metabolite aminomethyl phosphonic acid by gas chromatography-flame photometric detection," Journal of chromatography. A **1589**, 116–121 (2019).
12. R. Jiang, Y.-H. Pang, Q.-Y. Yang, *et al.*, "Copper porphyrin metal-organic framework modified carbon paper for electrochemical sensing of glyphosate," Sens. Actuators, B **358**, 131492 (2022).
13. S. Dovidauskas, I. A. Okada, and F. R. D. Santos, "Validation of a simple ion chromatography method for simultaneous determination of glyphosate, aminomethylphosphonic acid and ions of Public Health concern in water intended for human consumption," Journal of Chromatography A **1632**(0), 461603 (2020).
14. L. K. S. De Almeida, S. Chigome, N. Torto, *et al.*, "A novel colorimetric sensor strip for the detection of glyphosate in water," Sens. Actuators, B **206**, 357–363 (2015).
15. E. Junqué, P. Fernández, I. Filippi, *et al.*, "Determination of glyphosate and its derivative, aminomethylphosphonic acid, in human urine by gas chromatography coupled to tandem mass spectrometry and isotope pattern deconvolution," J. Chromatogr. Open **4**, 100087 (2023).
16. K. K. K. Gains, N. G. K. Roland, K. Y. Urbain, *et al.*, "Determination of the Glyphosate Content in Liquid and Dry Formulations by HPLC-UV: Pre-column Derivation with 9-Fluorenylmethyl Chloroformate (FMOC)," Chromatographia **85**(7), 655–664 (2022).
17. B. S. Clegg, G. R. Stephenson, and J. C. Hall, "Development of an enzyme-linked immunosorbent assay for the detection of glyphosate," J. Agric. Food Chem. **47**(12), 5031–5037 (1999).
18. M. T. Jacques, J. Bornhorst, M. V. Soares, *et al.*, "Reprotoxicity of glyphosate-based formulation in Caenorhabditis elegans is not due to the active ingredient only(Article)," Environ. Pollut. **252**, 1854–1862 (2019).
19. M. B. Elamin, S. M. A. Ali, A. Chrouda, *et al.*, "Green synthesis of gum arabic platinum nanoparticle: Electrochemical sensor application for glyphosate detection," Polym. Adv. Technol. **34**(11), 3407–3414 (2023).
20. A. I. Takahiro Morimoto and M. Tanimizu, "Simultaneous and sensitive analysis of glyphosate, glufosinate, and their metabolites in surface water by HPLC-ICP-MS/MS," ANAL. SCI. **39**(7), 1047–1052 (2023).
21. S. Lin, F. Wang, Y. Qu, *et al.*, "High-temperature measurement based on highly-sensitive miniature cascaded FPIs and the harmonic Vernier effect," Measurement **221**, 113456 (2023).
22. X. L. Hongxin Zhang, X. Zhou, P. Gong, *et al.*, "U-fiber-based biosensor for temperature-compensated acetylcholine-specific measurement," Opt. Lett. **48**(8), 2138–2141 (2023).
23. R. Singh, W. Zhang, X. Liu, *et al.*, "WaveFlex biosensor: MXene-immobilized W-shaped fiber-based LSPR sensor for highly selective tyramine detection," Opt. Laser Technol. **171**, 110357 (2024).
24. P. Bhatia and S. S. Verma, "Enhancement of LSPR properties of temperature-dependent gold nanoparticles," Mater. Today:. Proc. **78**, 871–876 (2023).
25. Z. Ma, X. Lv, W. Fang, *et al.*, "Au nanoparticle-based integrated microfluidic plasmonic chips for the detection of carcinoembryonic antigen in human serum," ACS Appl. Nano Mater. **5**(11), 17281–17292 (2022).
26. H. S. Mondal, M. Z. Hossain, and N. Birbilis, "A selective LSPR biosensor for molecular-level glycated albumin detection," Heliyon **9**(12), e22795 (2023).
27. S. Lee, S. H. Lee, B. Paulson, *et al.*, "Enhancement of local surface plasmon resonance (LSPR) effect by biocompatible metal clustering based on ZnO nanorods in Raman measurements," Spectrochim. Acta, Part A **204**, 203–208 (2018).
28. W. Zhang, R. Singh, F.-Z. Liu, *et al.*, "WaveFlex biosensor: a flexible-shaped plasmonic optical fiber sensor for histamine detection," IEEE Sens. J. **23**(19), 1 (2023).
29. O. F. Farag and E. Abdel-Fattah, "Synthesis and characterization PVA/plasma-functionalized MWCNTs nanocomposites films," J. Polym. Res. **30**(5), 183 (2023).

Optics EXPRESS

30. B. Hassan Pour, N. Haghnazari, F. Keshavarzi, *et al.*, "High sensitive electrochemical sensor for imatinib based on metal-organic frameworks and multiwall carbon nanotubes nanocomposite," Microchem. J. **165**, 106147 (2021).
31. A. Z. Hajjaj, K. N. Chappanda, N. M. Batra, *et al.*, "Miniature pressure sensor based on suspended MWCNT," Sens. Actuators, A **292**, 11–16 (2019).
32. Y. Wang, M. Ni, J. Chen, *et al.*, "An ultra-sensitive luteolin sensor based on Co-doped nitrogen-containing carbon framework/MoS_2−MWCNTs composite for natural sample detection," Electrochim. Acta **438**, 141534 (2023).
33. M. B. Souza, J. S. Santos, M. S. Pontes, *et al.*, "CeO_2 nanostructured electrochemical sensor for the simultaneous recognition of diethylstilbestrol and 17β-estradiol hormones," Sci. Total Environ. **805**, 150348 (2022).
34. M. A. Takte, N. N. Ingle, B. N. Dole, *et al.*, "A stable and highly-sensitive flexible gas sensor based on ceria (CeO_2) nano-cube decorated rGO nanosheets for selective detection of NO_2 at room temperature," Synth. Met. **297**, 117411 (2023).
35. A. Umar, T. Almas, A. A. Ibrahim, *et al.*, "An efficient chemical sensor based on CeO_2 nanoparticles for the detection of acetylacetone chemical(Article)," J. Electroanal. Chem. **864**, 114089 (2020).
36. M. Mylarappa, S. Chandruvasan, K. S. Harisha, *et al.*, "Development of coriander honey loaded CeO_2 for cyclic voltammetry, chemical sensor, dye purification, and antioxidant properties," J. Taiwan Inst. Chem. Eng. **152**, 105174 (2023).
37. Í. A. Costa, M. A. Gross, E. D. O. Alves, *et al.*, "An impedimetric e-tongue based on CeO_2-graphene oxide chemical sensors for detection of glyphosate and its potential interferents," J. Electroanal. Chem. **922**, 116719 (2022).
38. N. Dogra, M. Singh, A. Kumar, *et al.*, "Selective room-temperature ammonia sensing using CeO_2-multiwalled carbon nanotube composite," Appl. Phys. A **129**(1), 24 (2023).
39. Q. Fu, Y. Xie, F. Gao, *et al.*, "Signal-enhanced multi-core fiber-based WaveFlex biosensor for ultra-sensitive xanthine detection," Opt. Express **31**(26), 43178–43197 (2023).
40. G. Zhu, Y. Wang, Z. Wang, *et al.*, "Localized plasmon-based multicore fiber biosensor for acetylcholine detection," IEEE Trans. Instrum. Meas. **71**, 1–9 (2022).
41. X. Wang, Y. Wang, and Q. Ling, "Seven-core fiber embedded ultra-long period grating for curvature, torsion or temperature sensing," Opt. Commun. **536**, 129351 (2023).
42. W. Jin, W. Wang, J. Li, *et al.*, "A multi-angle torsion sensor based on seven-core fiber microcavity structure," Opt. Fiber Technol. **71**, 102932 (2022).
43. Z. Wang, R. Singh, C. A. F. Marques, *et al.*, "Taper-in-taper fiber structure-based LSPR sensor for alanine aminotransferase detection," Opt. Express **29**(26), 43793–43810 (2021).
44. S. V. Kergaravat, S. N. Fabiano, A. R. Soutullo, *et al.*, "Comparison of the performance analytical of two glyphosate electrochemical screening methods based on peroxidase enzyme inhibition(Article)," Microchem. J. **160**(Part A), 105654 (2021).
45. A. L.-C. Diego Morales-Urrea and E. M. Contreras, "Inactivation kinetics of horseradish peroxidase (HRP) by hydrogen peroxide," Sci. Rep. **13**(1), 13363 (2023).
46. Q. Zhang, G. Xu, L. Gong, *et al.*, "An enzyme-assisted electrochemiluminescent biosensor developed on order mesoporous carbons substrate for ultrasensitive glyphosate sensing," Electrochim. Acta **186**, 624–630 (2015).
47. A. J. Haes and R. P. V. Duyne, "A nanoscale optical biosensor: Sensitivity and selectivity of an approach based on the localized surface plasmon resonance spectroscopy of triangular silver nanoparticles," J. Am. Chem. Soc. **124**(35), 10596–10604 (2002).
48. X. Zhu, W. Liu, A. Sun, *et al.*, "Highly sensitive temperature and curvature sensor based on seven-core fiber," Opt. Lasers Eng. **169**, 107725 (2023).
49. J. Turkevich, P. C. Stevenson, and J. Hillier, "A study of the nucleation and growth processes in the synthesis of colloidal gold," Discuss. Faraday Soc. **11**, 55–75 (1951).
50. L. Wang, Y. Zhang, W. Zhang, *et al.*, "Two-dimensional microbend sensor based on the 2-core fiber with hump-shaped taper fiber structure," Opt. Fiber Technol. **52**, 101948 (2019).
51. R. S. Wen Zhang, Z. Wang, G. Li, *et al.*, "Humanoid shaped optical fiber plasmon biosensor functionalized with graphene oxide/multi-walled carbon nanotubes for histamine detection," Opt. Express **31**(7), 11788–11803 (2023).
52. A. Islam, F. Haider, R. Ahmmed Aoni, *et al.*, "Plasmonic photonic biosensor: in situ detection and quantification of SARS-CoV-2 particles," Opt. Express **30**(22), 40277–40291 (2022).
53. C. Qiu, L. Zhang, H. Li, *et al.*, "Development of a sensitive ZnO/CuO/Au electrochemical sensor for measuring glyphosate," Vacuum **214**, 112138 (2023).
54. S. V. Pranlekha Traiwatcharanon, M. Zacharias, and C. Wongchoosuk, "Sparked ZnO nanoparticles-based electrochemical sensor for onsite determination of glyphosate residues," Nanotechnology **34**(41), 415501 (2023).
55. Z. Z. Qianru Zhang, S. Xu, L. Da, *et al.*, "Enzyme-free and rapid visual quantitative detection for pesticide residues utilizing portable smartphone integrated paper sensor," J. Hazard. Mater. **436**, 129320 (2022).
56. Z. Fu, J. He, Y. Li, *et al.*, "A novel and ultrasensitive fluorescent probe derived from labeled carbon dots for recognitions of copper ions and glyphosate," Spectrochim. Acta, Part A **287**, 122052 (2023).
57. F. M. L. Bombardi, M. Muller, and J. L. Fabris, "U-shaped fiber sensor based on surface plasmon resonance of gold nanoparticles for measuring glyphosate in water," J. Lightwave Technol. 1–10 (2024).
58. A. Fernandez-Perez, B. Frijns, and A. Tourani-Rad, "Functionalized long period grating—plasmonic fiber sensor applied to the detection of glyphosate in water," J. Lightwave Technol. **36**(4), 863–870 (2018).